Draft version August 18, 2006
Preprint typeset using LaTeX style emulateapj v. 11/26/03

A DIRECT EMPIRICAL PROOF OF THE EXISTENCE OF DARK MATTER *

Douglas Clowe[1], Maruša Bradač[2], Anthony H. Gonzalez[3], Maxim Markevitch[4,5], Scott W. Randall[4], Christine Jones[4], and Dennis Zaritsky[1]

Draft version August 18, 2006

ABSTRACT

We present new weak lensing observations of 1E0657−558 ($z = 0.296$), a unique cluster merger, that enable a direct detection of dark matter, independent of assumptions regarding the nature of the gravitational force law. Due to the collision of two clusters, the dissipationless stellar component and the fluid-like X-ray emitting plasma are spatially segregated. By using both wide-field ground based images and HST/ACS images of the cluster cores, we create gravitational lensing maps which show that the gravitational potential does not trace the plasma distribution, the dominant baryonic mass component, but rather approximately traces the distribution of galaxies. An 8σ significance spatial offset of the center of the total mass from the center of the baryonic mass peaks cannot be explained with an alteration of the gravitational force law, and thus proves that the majority of the matter in the system is unseen.

Subject headings: Gravitational lensing – Galaxies: clusters: individual: 1E0657-558 – dark matter

1. INTRODUCTION

We have known since 1937 that the gravitational potentials of galaxy clusters are too deep to be caused by the detected baryonic mass and a Newtonian r^{-2} gravitational force law (Zwicky 1937). Proposed solutions either invoke dominant quantities of non-luminous "dark matter" (Oort 1932) or alterations to either the gravitational force law (Bekenstein 2004; Brownstein & Moffat 2006) or the particles' dynamical response to it (Milgrom 1983). Previous works aimed at distinguishing between the dark matter and alternative gravity hypotheses in galaxies (Buote et al. 2002; Hoekstra et al. 2004) or galaxy clusters (Gavazzi 2002; Pointecouteau & Silk 2005) have used objects in which the visible baryonic and hypothesized dark matter are spatially coincident, as in most of the Universe. These works favor the dark matter hypothesis, but their conclusions were necessarily based on non-trivial assumptions such as symmetry, the location of the center of mass of the system, and/or hydrostatic equilibrium, which left room for counterarguments. The actual existence of dark matter can only be confirmed either by a laboratory detection or, in an astronomical context, by the discovery of a system in which the observed baryons and the inferred dark matter are spatially segregated. An ongoing galaxy cluster merger is such a system.

Given sufficient time, galaxies (whose stellar component makes up $\sim 1-2\%$ of the mass (Kochanek et al. 2003) under the assumption of Newtonian gravity), plasma ($\sim 5-15\%$ of the mass (Allen et al. 2002; Vikhlinin et al. 2006)), and any dark matter in a typical cluster acquire similar, centrally-symmetric spatial distributions tracing the common gravitational potential. However, during a merger of two clusters, galaxies behave as collisionless particles, while the fluid-like X-ray emitting intracluster plasma experiences ram pressure. Therefore, in the course of a cluster collision, galaxies spatially decouple from the plasma. We clearly see this effect in the unique cluster 1E0657−558 (Tucker et al. 1998).

The cluster has two primary galaxy concentrations separated by 0.72 Mpc on the sky, a less massive ($T \sim 6$ keV) western subcluster and a more massive ($T \sim 14$ keV) eastern main cluster (Markevitch et al. 2002). Both concentrations have associated X-ray emitting plasma offset from the galaxies toward the center of the system. The X-ray image also shows a prominent bow shock on the western side of the western plasma cloud, indicating that the subcluster is currently moving away from the main cluster at ∼4700 km/s. As the line-of-sight velocity difference between the components is only ∼ 600 km/s (Barrena et al. 2002), the merger must be occurring nearly in the plane of the sky and the cores passed through each other ∼ 100 Myr ago.

Two galaxy concentrations that correspond to the main cluster and the smaller subcluster have moved ahead of their respective plasma clouds that have been slowed by ram pressure. This phenomenon provides an excellent setup for our simple test. In the absence of dark matter, the gravitational potential will trace the dominant visible matter component, which is the X-ray plasma. If, on the other hand, the mass is indeed domi-

*BASED ON OBSERVATIONS MADE WITH THE NASA/ESA HUBBLE SPACE TELESCOPE, OBTAINED AT THE SPACE TELESCOPE SCIENCE INSTITUTE, WHICH IS OPERATED BY THE ASSOCIATION OF UNIVERSITIES FOR RESEARCH IN ASTRONOMY, INC., UNDER NASA CONTRACT NAS 5–26555, UNDER PROGRAM 10200, THE 6.5 METER MAGELLAN TELESCOPES LOCATED AT LAS CAMPANAS OBSERVATORY, CHILE, THE ESO TELESCOPES AT THE PARANAL OBSERVATORIES UNDER PROGRAM IDS 72.A-0511, 60.A-9203, AND 64.O-0332, AND WITH THE NASA CHANDRA X-RAY OBSERVATORY, OPERATED BY THE SMITHSONIAN ASTROPHYSICS OBSERVATORY UNDER CONTRACT TO NASA.

Electronic address: dclowe@as.arizona.edu
[1] Steward Observatory, University of Arizona, 933 N Cherry Ave, Tucson, AZ 85721
[2] Kavli Institute for Particle Astrophysics and Cosmology, P.O. Box 20450, MS29, Stanford, CA 94309
[3] Department of Astronomy, University of Florida, 211 Bryant Space Science Center, Gainesville, FL 32611
[4] Harvard-Smithsonian Center for Astrophysics, 60 Garden St., Cambridge, MA 02138
[5] Also Space Research Institute, Russian Acad. Sci., Profsoyuznaya 84/32, Moscow 117997, Russia

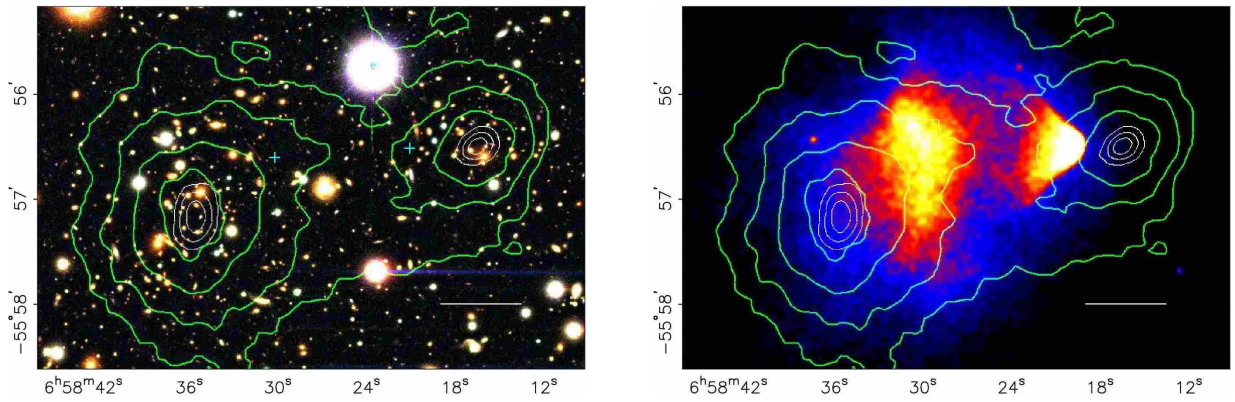

FIG. 1.— Shown above in the top panel is a color image from the Magellan images of the merging cluster 1E0657−558, with the white bar indicating 200 kpc at the distance of the cluster. In the bottom panel is a 500 ks Chandra image of the cluster. Shown in green contours in both panels are the weak lensing κ reconstruction with the outer contour level at $\kappa = 0.16$ and increasing in steps of 0.07. The white contours show the errors on the positions of the κ peaks and correspond to 68.3%, 95.5%, and 99.7% confidence levels. The blue +s show the location of the centers used to measure the masses of the plasma clouds in Table 2.

nated by collisionless dark matter, the potential will trace the distribution of that component, which is expected to be spatially coincident with the collisionless galaxies. Thus, by deriving a map of the gravitational potential, one can discriminate between these possibilities. We published an initial attempt at this using an archival VLT image (Clowe et al. 2004); here we add three additional optical image sets which allows us to increase the significance of the weak lensing results by more than a factor of 3.

In this paper, we measure distances at the redshift of the cluster, $z = 0.296$, by assuming an $\Omega_{\rm m} = 0.3, \lambda = 0.7, H_0 = 70$km/s/Mpc cosmology which results in 4.413 kpc/$''$ plate-scale. None of the results of this paper are dependent on this assumption; changing the assumed cosmology will result in a change of the distances and absolute masses measured, but the relative masses of the various structures in each measurement remain unchanged.

2. METHODOLOGY AND DATA

We construct a map of the gravitational potential using weak gravitational lensing (Mellier 1999; Bartelmann & Schneider 2001), which measures the distortions of images of background galaxies caused by the gravitational deflection of light by the cluster's mass. This deflection stretches the image of the galaxy preferentially in the direction perpendicular to that of the cluster's center of mass. The imparted ellipticity is typically comparable to or smaller than that intrinsic to the galaxy, and thus the distortion is only measurable statistically with large numbers of background galaxies. To do this measurement, we detect faint galaxies on deep optical images and calculate an ellipticity from the second moment of their surface brightness distribution, correcting the ellipticity for smearing by the point spread function (corrections for both anisotropies and smearing are obtained using an implementation of the KSB technique (Kaiser et al. 1995) discussed in Clowe et al. (2006)). The corrected ellipticities are a direct, but noisy, measurement of the reduced shear $\vec{g} = \vec{\gamma}/(1-\kappa)$. The shear $\vec{\gamma}$ is the amount of anisotropic stretching of the galaxy image. The convergence κ is the shape-independent increase in the size of the galaxy image. In Newtonian gravity, κ is equal to the surface mass density of the lens divided by a scaling constant. In non-standard gravity models, κ is no longer linearly related to the surface density but is instead a non-local function that scales as the mass raised to a power less than one for a planar lens, reaching the limit of one half for constant acceleration (Mortlock & Turner 2001; Zhao et al. 2006). While one can no longer directly obtain a map of the surface mass density using the distribution of κ in non-standard gravity models, the locations of the κ peaks, after adjusting for the extended wings, correspond to the locations of the surface mass density peaks.

Our goal is thus to obtain a map of κ. One can combine derivatives of $\vec{g}$ to obtain (Schneider 1995; Kaiser 1995)

$$\nabla \ln(1-\kappa) = \frac{1}{1-g_1^2-g_2^2} \begin{pmatrix} 1+g_1 & g_2 \\ g_2 & 1-g_1 \end{pmatrix} \begin{pmatrix} g_{1,1}+g_{2,2} \\ g_{2,1}-g_{1,2} \end{pmatrix},$$

which is integrated over the data field and converted into a two-dimensional map of κ. The observationally unconstrained constant of integration, typically referred to as the "mass-sheet degeneracy," is effectively the true mean of $\ln(1-\kappa)$ at the edge of the reconstruction. This method does, however, systematically underestimate κ in the cores of massive clusters. This results in a slight increase to the centroiding errors of the peaks, and our measurements of κ in the peaks of the components are only lower bounds.

For 1E0657−558, we have accumulated an exceptionally rich optical dataset, which we will use here to measure $\vec{g}$. It consists of the four sets of optical images shown in Table 1 and the VLT image set used in Clowe et al. (2004); the additional images significantly increase the maximum resolution obtainable in the κ reconstructions due to the increased number of background galaxies, particularly in the area covered by the ACS images, with which we measure the reduced shear. We reduce each image set independently and create galaxy catalogs with 3 passband photometry. The one exception is the single passband HST pointing of main cluster, for which we measure colors from the Magellan images. Because it is not feasible to measure redshifts for all galaxies in the field, we select likely background galaxies using magnitude and color cuts ($m_{814} > 22$ and not in the rhombus defined by $0.5 < m_{606} - m_{814} < 1.5$,

Table 1. Optical Imaging Sets

Instrument	Date of Obs.	FoV	Passband	$t_{\rm exp}$ (s)	$m_{\rm lim}$	$n_{\rm d}$ ($'^{-2}$)	seeing
2.2m ESO/MPG	01/2004	$34' \times 34'$	R	14100	23.9	15	$0\farcs8$
Wide Field Imager	01/2004		B	6580			$1\farcs0$
	01/2004		V	5640			$0\farcs9$
6.5m Magellan	01/15/2004	$8'$ radius	R	10800	25.1	35	$0\farcs6$
IMACS	01/15/2004		B	2700			$0\farcs9$
	01/15/2004		V	2400			$0\farcs8$
HST ACS	10/21/2004	$3\farcm5 \times 3\farcm5$	F814W	4944	27.6	87	$0\farcs12$
subcluster	10/21/2004		F435W	2420			$0\farcs12$
	10/21/2004		F606W	2336			$0\farcs12$
main cluster	10/21/2004	$3\farcm5 \times 3\farcm5$	F606W	2336	26.1	54	$0\farcs12$

Note. — Limiting magnitudes for completion are given for galaxies and measured by where the number counts depart from a power law. All image sets had objects detected in the reddest passband available.

$m_{435} - m_{606} > 1.5 * (m_{606} - m_{814}) - 0.25$, and $m_{435} - m_{606} < 1.6*(m_{606} - m_{814}) + 0.4$ for the ACS images; similar for the other image sets) that were calibrated with photometric redshifts from the HDF-S (Fontana et al. 1999). Each galaxy has a statistical weight based on its significance of detection in the image set (Clowe et al. 2006), and the weights are normalized among catalogs by comparing the rms reduced shear measured in a region away from the cores of the cluster common to all five data sets. To combine the catalogs, we adopt a weighted average of the reduced shear measurements and appropriately increase the statistical weight of galaxies that occur in more than one catalog.

3. ANALYSIS

We use the combined catalog to create a two-dimensional κ reconstruction, the central portion of which is shown in Fig. 1. Two major peaks are clearly visible in the reconstruction, one centered $7\farcs1$ east and $6\farcs5$ north of the subcluster's brightest cluster galaxy (BCG) and detected at 8σ significance (as compared to 3σ in (Clowe et al. 2004)), and one centered $2\farcs5$ east and $11\farcs5$ south of the northern BCG in the main cluster ($21\farcs2$ west and $17\farcs7$ north of the southern BCG) detected at 12σ. We estimate centroid uncertainties by repeating bootstrap samplings of the background galaxy catalog, performing a κ reconstruction with the resampled catalogs, and measuring the centroid of each peak. Both peaks are offset from their respective BCG by $\sim 2\sigma$, but are within 1σ of the luminosity centroid of the respective component's galaxies (both BCGs are slightly offset from the center of galaxy concentrations). Both peaks are also offset at $\sim 8\sigma$ from the center of mass of their respective plasma clouds. They are skewed toward the plasma clouds, which is expected because the plasma contributes about 1/10th of the total cluster mass (Allen et al. 2002; Vikhlinin et al. 2006) (and a higher fraction in non-standard gravity models without dark matter). The skew in each κ peak toward the X-ray plasma is significant even after correcting for the overlapping wings of the other peak, and the degree of skewness is consistent with the X-ray plasma contributing $14\%^{+16\%}_{-14\%}$ of the observed κ in the main cluster and $10\%^{+30\%}_{-10\%}$ in the subcluster (see Table 2). Because of the large size of the reconstruction ($34'$ or 9 Mpc on a side), the change in κ due to the mass-sheet degeneracy should be less than 1% and any systematic effects on the centroid and skewness of the peaks are much smaller than the measured error bars.

The projected cluster galaxy stellar mass and plasma mass within 100 kpc apertures centered on the BCGs and X-ray plasma peaks are shown in Table 2. This aperture size was chosen as smaller apertures had significantly higher kappa measurement errors and larger apertures resulted in significant overlap of the apertures. Plasma masses were computed from a multicomponent 3-dimensional cluster model fit to the Chandra X-ray image (details of this fit will be given elsewhere). The emission in the Chandra energy band (mostly optically-thin thermal bremsstrahlung) is proportional to the square of the plasma density, with a small correction for the plasma temperature (also measured from the X-ray spectra), which gives the plasma mass. Because of the simplicity of this cluster's geometry, especially at the location of the subcluster, this mass estimate is quite robust (to a 10% accuracy).

Stellar masses are calculated from the I-band luminosity of all galaxies equal in brightness or fainter than the component BCG. The luminosities were converted into mass assuming (Kauffmann et al. 2003) $M/L_I = 2$. The assumed mass-to-light ratio is highly uncertain (can vary between 0.5 and 3) and depends on the history of recent star formation of the galaxies in the apertures; however even in the case of an extreme deviation, the X-ray plasma is still the dominant baryonic component in all of the apertures. The quoted errors are only the errors on measuring the luminosity and do not include the uncertainty in the assumed mass-to-light ratio. Because we did not apply a color selection to the galaxies, these measurements are an upper limit on the stellar mass as they include contributions from galaxies not affiliated with the cluster.

The mean κ at each BCG was calculated by fitting a two peak model, each peak circularly symmetric, to the reconstruction and subtracting the contribution of the other peak at that distance. The mean κ for each plasma cloud is the excess κ after subtracting off the values for both peaks.

The total of the two visible mass components of the subcluster is greater by a factor of 2 at the plasma peak

Table 2. Component Masses

Component	RA (J2000)	Dec (J2000)	$M_{\rm X}(10^{12}M_\odot)$	$M_*(10^{12}M_\odot)$	$\bar{\kappa}$
Main cluster BCG	06 : 58 : 35.3	−55 : 56 : 56.3	5.5 ± 0.6	0.54 ± 0.08	0.36 ± 0.06
Main cluster plasma	06 : 58 : 30.2	−55 : 56 : 35.9	6.6 ± 0.7	0.23 ± 0.02	0.05 ± 0.06
Subcluster BCG	06 : 58 : 16.0	−55 : 56 : 35.1	2.7 ± 0.3	0.58 ± 0.09	0.20 ± 0.05
Subcluster plasma	06 : 58 : 21.2	−55 : 56 : 30.0	5.8 ± 0.6	0.12 ± 0.01	0.02 ± 0.06

Note. — All values are calculated by averaging over an aperture of 100 kpc radius around the given position (marked with blue +s for the centers of the plasma clouds in Fig 1). $\bar{\kappa}$ measurements for the plasma clouds are the residual left over after subtraction of circularly symmetric profiles centered on the BCGs.

than at the BCG; however, the center of the lensing mass is located near the BCG. The difference of the baryonic mass between these two positions would be even greater if we excluded a contribution of the non-peaked plasma component between the shock front and the subcluster. For the main cluster, we see the same effect, although the baryonic mass difference is smaller. Note that both the plasma mass and the stellar mass are determined directly from the X-ray and optical images, respectively, independently of any gravity or dark matter models.

4. DISCUSSION

A key limitation of the gravitational lensing methodology is that it only produces a two-dimensional map of κ, and hence raises the possibility that structures seen in the map are caused by physically unrelated masses along the line-of-sight. Because the background galaxies reside at a mean $z \sim 1$, structures capable of providing a significance amount of κ must lie at $z \lesssim 0.8$. By comparing the measured shear for galaxies divided into crude redshift bins using photometric redshifts (Wittman et al. 2003), we further limit the redshift of the lensing objects to $0.18 < z < 0.39$. This range is consistent with the cluster redshift, but corresponds to a large volume in which a structure unassociated with the cluster could exist and be projected onto the lensing map. However, the number density of structures with these lensing strengths in blank field surveys is $\sim 10^{-3}$ arcmin^{-2} for the subcluster (Wittman et al. 2006), and an order of magnitude less for the main cluster, resulting in a $\sim 10^{-7}$ probability of having two structures within a square arcminute of the observed cluster cores. Further, all such lenses observed in these cosmic shear surveys are clusters with enough plasma and galaxies to be easily observable. There is no evidence, however, in our deep imaging for additional cluster sized concentrations of galaxies or of plasma hotter than $T \sim 0.5$ keV (the lower bound of the Chandra energy band) near the observed lensing structures.

Another alternate explanation of the lensing signal is related to the fact that clusters form at the intersections of matter filaments (Bond et al. 1996). In principle, one could imagine two line-of-sight filaments of intergalactic gas (too cool to be visible with Chandra and too diffuse to have cooled into stars) extending from the cluster at the locations of the weak lensing peaks. To explain the measured surface mass density, such filaments would have to be several Megaparsecs long, very narrow, and oriented exactly along the line of sight. The probability of such an orientation for two such filaments in the field is $\sim 10^{-6}$. Further, because the two cluster components are moving at a relative transverse velocity of 4700 km/s compared to the typical peculiar velocities in the CMB frame of a few hundred km/s, the filaments could coincide so exactly with each of the BCGs only by chance. This is an additional factor of $\sim 10^{-5}$ reduction in probability. While such projections become more important in non-standard gravity models because in such models the thin lens approximation breaks down (Mortlock & Turner 2001) and structures with a given surface density produce a greater amount of lensing the more they are extended along the line-of-sight, two such projections would still have a $\ll 10^{-8}$ probability. Finally, we mention that two other merging clusters, MS1054−03 (Jee et al. 2005) and A520 (in preparation), exhibit similar offsets between the peaks of the lensing and baryonic mass, although based on lensing reconstructions with lower spatial resolution and less clear-cut cluster geometry.

A final possibility is that some alternative gravity models may be able to suppress the lensing potential of the central peak in a multiple-peak system, as in Angus et al. (2006). That work used a model of a gas disk located between two symmetric mass concentrations representing the galaxy subclusters. In their κ map, derived in the TeVeS framework (Bekenstein 2004), the relative signal from this disk may be suppressed, but would still be easily visible with the noise levels of our reconstruction. Our κ map, however, has no evidence of any mass concentration between the two galaxy subclusters other than the small perturbations consistent with the gas mass contribution in Newtonian gravity. Furthermore, such a suppression has also only been shown to work for symmetric systems which have the central peak directly between the two outer peaks. In 1E0657−558, however, the X-ray plasma, which would provide the central peak, lies north of the line connecting the two κ peaks. Further, the absolute κ levels of the peaks observed in 1E0657−558 are in good agreement with those in systems with similar velocity dispersions and X-ray temperatures (e.g. Clowe & Schneider 2002) which have the gas and the galaxies coincident. The κ-to-light ratios are also consistent with those in normal clusters with coincident gas and galaxies. Therefore one would need to not only suppress the inner peak in the κ map relative to the two outer peaks in this system, but also enhance the strength of the outer peaks to make up for the missing plasma mass.

Any non-standard gravitational force that scales with baryonic mass will fail to reproduce these observations.

The lensing peaks require unseen matter concentrations that are more massive than and offset from the plasma. While the existence of dark matter removes the primary motivation for alternative gravity models, it does not preclude non-standard gravity. The scaling relation between κ and surface mass density, however, has important consequences for models that mix dark matter with non-Newtonian gravity: to achieve the $\sim 7:1$ ratio in κ between the dark matter + galaxy component and the plasma component (Table 2), the true ratio of mass would be even higher (as high as 49:1 for a constant acceleration model; although MOND (Milgrom 1983) would not reach this ratio as the dark matter density would become high enough to shift the acceleration into the quasi-Newtonian regime), making the need for dark matter even more acute. Such high concentrations of dark matter, however, are extremely unlikely based on the measured X-ray plasma temperatures (Markevitch et al. 2002) and cluster galaxy velocity dispersions (Barrena et al. 2002).

The spatial separation of the dominant baryonic component in a galaxy cluster from the hypothesized dark matter produced during a cluster merger has enabled us to directly compare the dark matter hypothesis to one with only visible matter but a modified law of gravity. The observed displacement between the bulk of the baryons and the gravitational potential proves the presence of dark matter for the most general assumptions regarding the behavior of gravity.

We wish to thank Bhuvnesh Jain, Hongsheng Zhao, and Peter Schneider for useful discussions. This work was supported by NASA through grant number LTSA04-0000-0041 (DC and DZ). Support for program 10200 was provided by NASA through grant GO-10200.01 from the Space Telescope Science Institute, which is operated by the Association of Universities for Research in Astronomy, Inc., under NASA contract NAS 5-26555. MB acknowledges support from the NSF grant AST-0206286. MM acknowledges support from Chandra grant GO4-5152X.

REFERENCES

Allen, S. W., Schmidt, R. W., & Fabian, A. C. 2002, MNRAS, 334, L11
Angus, G. W., Famaey, B., & Zhao, H. S. 2006, MNRAS, in press
Barrena, R., Biviano, A., Ramella, M., Falco, E. E., & Seitz, S. 2002, A&A, 386, 816
Bartelmann, M. & Schneider, P. 2001, Phys. Rep., 340, 291
Bekenstein, J. D. 2004, Phys. Rev. D, 70, 083509
Bond, J. R., Kofman, L., & Pogosyan, D. 1996, Nature, 380, 603
Brownstein, J. R. & Moffat, J. W. 2006, MNRAS, 367, 527
Buote, D. A., Jeltema, T. E., Canizares, C. R., & Garmire, G. P. 2002, ApJ, 577, 183
Clowe, D. & Schneider, P. 2002, A&A, 395, 385
Clowe, D., Gonzalez, A., & Markevitch, M. 2004, ApJ, 604, 596
Clowe, D. et al. 2006, A&A, 451, 395
Fontana, A. et al. 1999, A&A, 343, L19
Gavazzi, R. 2002, New Astronomy Review, 46, 783
Hoekstra, H., Yee, H. K. C., & Gladders, M. D. 2004, ApJ, 606, 67
Jee, M. J., White, R. L., Ford, H. C., Blakeslee, J. P., Illingworth, G. D., Coe, D. A., & Tran, K.-V. H. 2005, ApJ, 634, 813
Kaiser, N. 1995, ApJ, 439, L1
Kaiser, N., Squires, G., & Broadhurst, T. 1995, ApJ, 449, 460
Kauffmann, G. et al. 2003, MNRAS, 341, 33
Kochanek, C. S., White, M., Huchra, J., Macri, L., Jarrett, T. H., Schneider, S. E., & Mader, J. 2003, ApJ, 585, 161
Markevitch, M., Gonzalez, A. H., David, L., Vikhlinin, A., Murray, S., Forman, W., Jones, C., & Tucker, W. 2002, ApJ, 567, L27
Mellier, Y. 1999, ARA&A, 37, 127
Milgrom, M. 1983, ApJ, 270, 365
Mortlock, D. J. & Turner, E. L. 2001, MNRAS, 327, 557
Oort, J. 1932, Bull. Astron. Inst. Netherlands, 6, 249
Pointecouteau, E. & Silk, J. 2005, MNRAS, 364, 654
Schneider, P. 1995, A&A, 302, 639
Tucker, W. et al. 1998, ApJ, 496, L5
Vikhlinin, A., Kravtsov, A., Forman, W., Jones, C., Markevitch, M., Murray, S. S., & Van Speybroeck, L. 2006, ApJ, 640, 691
Wittman, D., Dell'Antonio, I. P., Hughes, J. P., Margoniner, V. E., Tyson, J. A., Cohen, J. G., & Norman, D. 2006, ApJ, 643, 128
Wittman, D., Margoniner, V. E., Tyson, J. A., Cohen, J. G., Becker, A. C., & Dell'Antonio, I. P. 2003, ApJ, 597, 218
Zhao, H., Bacon, D., Taylor, A., & Horne, K. 2006, MNRAS, 368, 171
Zwicky, F. 1937, ApJ, 86, 217